

# Rotating mixed $^3\text{He}$ - $^4\text{He}$ nanodroplets

Martí Pi,<sup>1,2,\*</sup> Francesco Ancilotto,<sup>3,4</sup> José María Escartín,<sup>5</sup> Ricardo Mayol,<sup>1,2</sup> and Manuel Barranco<sup>1,2,6</sup>

<sup>1</sup>*Departament FQA, Facultat de Física, Universitat de Barcelona. Diagonal 645, 08028 Barcelona, Spain*

<sup>2</sup>*Institute of Nanoscience and Nanotechnology (IN2UB), Universitat de Barcelona, Barcelona, Spain.*

<sup>3</sup>*Dipartimento di Fisica e Astronomia “Galileo Galilei” and CNISM,*

*Università di Padova, via Marzolo 8, 35122 Padova, Italy*

<sup>4</sup>*CNR-IOM Democritos, via Bonomea, 265 - 34136 Trieste, Italy*

<sup>5</sup>*Institut de Química Teòrica i Computacional, Universitat de Barcelona,*

*Carrer de Martí i Franquès 1, 08028 Barcelona, Spain.*

<sup>6</sup>*Université Toulouse 3, Laboratoire des Collisions, Agrégats et Réactivité,*

*IRSAMC, 118 route de Narbonne, F-31062 Toulouse Cedex 09, France*

(Dated: June 14, 2022)

Mixed  $^3\text{He}$ - $^4\text{He}$  droplets created by hydrodynamic instability of a cryogenic fluid-jet may acquire angular momentum during their passage through the nozzle of the experimental apparatus. These free-standing droplets cool down to very low temperatures undergoing isotopic segregation, developing a nearly pure  $^3\text{He}$  crust surrounding a very  $^4\text{He}$ -rich superfluid core. Here, the stability and appearance of rotating mixed helium droplets are investigated using Density Functional Theory for an isotopic composition that highlights, with some marked exceptions related to the existence of the superfluid inner core, the analogies with viscous rotating droplets.

Ordinary liquids are known to form droplets held together by surface tension. When they are set into rotation, their spherical shape experiences large deformations, evolving from oblate to prolate and 2-lobed, eventually fissioning if the rotational velocity is large enough.<sup>3</sup> Experiments carried out by Plateau on olive oil droplets immersed in a mixture of water and alcohol with nearly the same density, disclosed the sequence of droplet shapes as the angular velocity of the rotating shaft to which they were attached increased.<sup>2</sup> The appearance and stability of, e.g., rotating celestial bodies,<sup>3</sup> atomic nuclei<sup>4</sup> and tektites,<sup>5</sup> to cite some quite different objects, has been found to bear similarities with rotating classical droplets, adding an extrinsic interest to their study.

Helium, in its two isotopes  $^4\text{He}$  and  $^3\text{He}$ , is the only element in nature that may remain liquid and form droplets at temperatures ( $T$ ) close to absolute zero.<sup>6</sup> Both isotopes may be superfluid, with normal-to-superfluid transition temperatures of 2.17 K ( $^4\text{He}$ ) and 2.7 mK ( $^3\text{He}$ ). At the temperatures of helium droplets experiments, 0.37 K for  $^4\text{He}$ <sup>7</sup> and 0.15 K for  $^3\text{He}$ ,<sup>8</sup>  $^3\text{He}$  is a normal fluid whereas  $^4\text{He}$  is superfluid. They constitute an ideal test-ground to study how superfluidity affects rotation, as they are isolated quantum systems formed by atoms subject to the same bare interaction.

Rotating superfluid  $^4\text{He}$  droplets made of  $N_4 = 10^8 - 10^{10}$  atoms, produced by hydrodynamic instability of a cryogenic fluid-jet, have been studied by coherent x-rays scattering from a free-electron laser,<sup>9</sup> revealing the presence of vortex lattices through the observation of Bragg patterns produced by Xe clusters captured by the vortex lines. Coherent diffractive imaging experiments using extreme ultraviolet pulses have also been carried out, aimed at providing informations about the droplet shapes.<sup>10</sup> Surprisingly, these studies have shown that superfluid  $^4\text{He}$  droplets follow the same shape sequence of rotating viscous droplets made of normal fluid. It has been shown

that this is due to the presence of quantized vortices and capillary waves, whose interplay confers to the superfluid droplet the appearance of a classical rotating object.<sup>1,12</sup> Until now, a deeper knowledge of how superfluid droplets rotate has been hampered by the experimental difficulty of determining their angular momentum, which is usually unknown.<sup>12</sup> This prevents a detailed comparison with theoretical models and the disclosure of the precise quantum nature of such rotation. Similar studies have been conducted very recently for rotating pure  $^3\text{He}$  droplets.<sup>13</sup> These droplets are non-superfluid and, as shown by Density Functional Theory (DFT) calculations,<sup>5</sup> behave very much as classical rotating droplets.

In liquid helium mixtures characterized by the  $^3\text{He}$  fraction  $x_3 = N_3/N$ , with  $N = N_3 + N_4$ , the normal-to-superfluid transition temperature decreases with increasing  $x_3$ .<sup>15</sup> At low  $T$ , the mixture undergoes a two-phase separation where a pure  $^3\text{He}$  phase coexists with a very  $^4\text{He}$ -rich mixture.<sup>15</sup> These properties are transferred to the mixed droplets, which at the experimental  $T$  –sensibly that of pure  $^3\text{He}$  droplets<sup>16</sup>– experience a two-phase separation yielding a core-shell structure, with a crust made of  $^3\text{He}$  atoms in the normal state and a superfluid core mostly made of  $^4\text{He}$  atoms.<sup>17</sup> This segregation has been instrumental in finding the minimum number of  $^4\text{He}$  atoms needed to display superfluidity.<sup>16</sup>

The ability of forming self-bound isolated droplets made of a superfluid core enveloped by a normal fluid shell is a unique characteristic of liquid helium mixtures at very low temperatures. Indeed, Bose-Einstein condensates (BEC) immersed in a Fermi sea have been observed,<sup>18</sup> but these systems are not self-bound, and only exist confined by an external trap to which the droplets adapt their shape; self-bound droplets made of mixtures of bosonic cold gases have been also observed,<sup>19,20</sup> and self-bound Bose-Fermi droplets have been studied theoretically.<sup>21</sup> However, these cold-gas

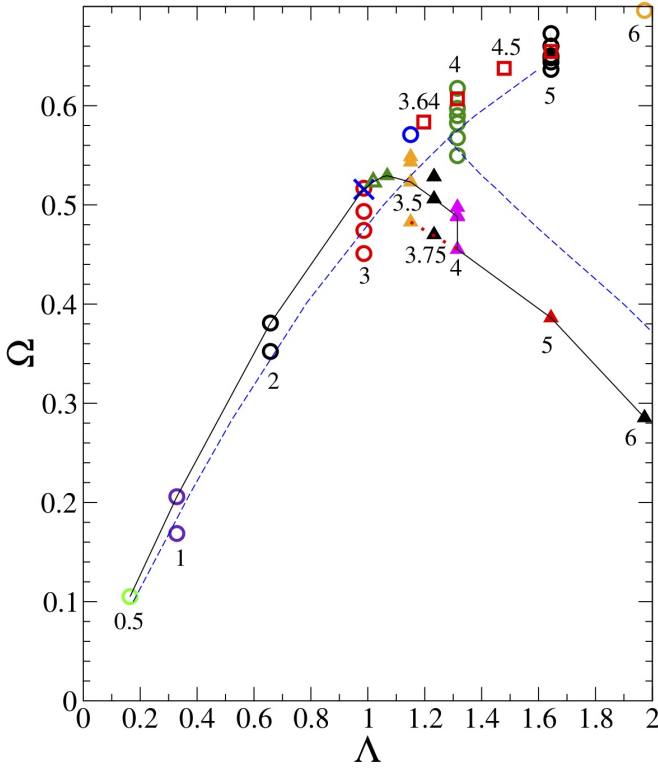


FIG. 1: Dimensionless angular velocity  $\Omega$  vs. dimensionless angular momentum  $\Lambda$ . The numbers close to the symbols indicate the  $\mathcal{L}$  value. Referring to the appearance of the outer surface of the  ${}^3\text{He}$  shell: open circles, oblate configurations [ $\Omega(\Lambda)$  rising branch]; triangles, prolate configurations [ $\Omega(\Lambda)$  falling branch]. Open squares, 3-lobed  ${}^4\text{He}$  core configurations. The cross indicates the oblate-to-prolate bifurcation point. The solid black line—drawn as a guide to the eye—connects the stable configurations for given  $\mathcal{L}$ , and the dotted red line shows the region of metastable fissioned  ${}^4\text{He}$  core configurations. The dashed blue line is the DFT result for pure  ${}^3\text{He}$  droplets.<sup>5</sup>

mixtures do not exist as phase-separated Bose-Fermi droplets, as they must remain in a mixed configuration to be self-bound.<sup>22</sup>

The mixed normal fluid-superfluid structure of  ${}^3\text{He}$ - ${}^4\text{He}$  droplets is expected to affect their structural properties as they are set into rotation. A recent study addresses theoretically the classical rotation of droplets made of two immiscible viscous fluids.<sup>6</sup> When one component is superfluid, as in the case studied here, then a quantum description is in order. We provide here such description.

## Results

We describe the stability and shape transitions of mixed He droplets within the DFT approach<sup>17</sup> taking as case of study a  ${}^4\text{He}_{1500}$ - ${}^3\text{He}_{6000}$  droplet ( $x_3 = 80\%$ ). The size and composition of this droplet, which can be seen

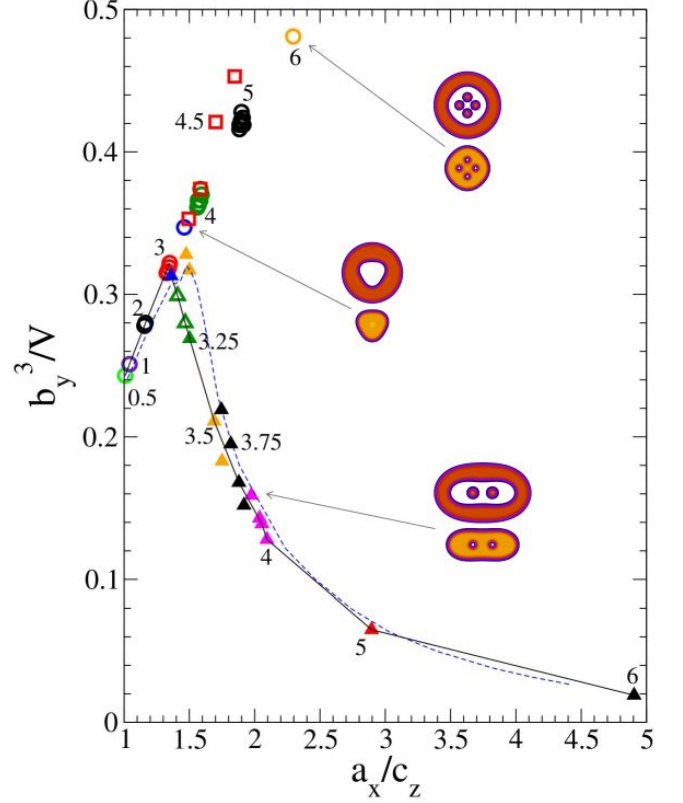


FIG. 2: Referring to the appearance of the outer surface of the  ${}^3\text{He}$  shell,  $b_y^3/V$  ratio vs.  $a_x/c_z$ , where  $V$  is the volume of the spherical droplet. Symbols and lines have the same meaning as in Fig. 1. The numbers close to the symbols indicate the  $\mathcal{L}$  value. The pictograms represent calculated  ${}^3\text{He}$  (top) and  ${}^4\text{He}$  (bottom) 2D densities for selected configurations.

in Supplementary Fig. 1, have been chosen (within the limitations imposed by the unavoidable computational cost of the calculations) for physical reasons: a thick  ${}^3\text{He}$  crust is needed to model a deformable container inside which the superfluid  ${}^4\text{He}$  core may undergo different shape transitions; a thin crust would just adapt to the deforming core and one should not expect a phenomenology much different from that of pure  ${}^4\text{He}$  droplets.<sup>1</sup> At the same time, the superfluid  ${}^4\text{He}$  inner droplet must be large enough to host a number of quantized vortices.<sup>1</sup> In superfluid liquid helium mixtures the vortex cores are filled with  ${}^3\text{He}$  and, depending on  $x_3$ , their radius can be up to five times larger than for pure  ${}^4\text{He}$ ,<sup>24</sup> as shown in Supplementary Fig. 2. For the chosen  $N_4$  value, the number of vortices ( $n_v$ ) is expected to be small.

The calculations have been carried out as a function of the angular momentum per atom around the rotation  $z$ -axis,  $\mathcal{L} = (L_3 + L_4)/N = \mathcal{L}_3 + \mathcal{L}_4$ , expressed in  $\hbar$  units throughout this work. For a given  $\mathcal{L}$ , the stable configuration is that with the lowest energy including the rotational energy (Routhian).<sup>3</sup>

We characterize the appearance of the  ${}^4\text{He}$  core and

$^3\text{He}$  crust by the distance of their sharp surfaces (defined, for each isotope, by the locus at which the density equals that of the bulk liquid divided by two<sup>1,5</sup>) to the center of mass of the droplet, denoting the distances along the  $x, y$  and  $z$  axes as  $a_x$ ,  $b_y$  and  $c_z$ , respectively. Dimensionless angular momentum  $\Lambda$  and angular velocity  $\Omega$  variables have been defined in Supplementary Section 2. As in pure droplets,<sup>3-5,12</sup> these variables are very useful to scale the results to droplets of different size for a given composition.<sup>6</sup>

The detailed energetics and morphologic characteristics of rotating mixed helium droplets are collected in Figs. 1-4 and Supplementary Table 1. Figure 1 shows the stability diagram and constitutes the main result of this work. Figure 2 provides information on the shapes of the droplets through relationships between the geometrical parameters  $a_x$ ,  $b_y$ , and  $c_z$  that characterize the shape of the outer  $^3\text{He}$  surface.<sup>5,10</sup> Lastly, Fig. 3 connects the shapes of the droplets with the dimensionless angular momentum  $\Lambda$ .

Our study has unveiled a rich variety of stable and metastable configurations. As  $\Lambda$  increases from zero, the  $^3\text{He}$  crust becomes oblate as it happens in normal fluids.<sup>3</sup> At variance, the superfluid  $^4\text{He}$  core remains spherical, becoming axisymmetric only when the angular momentum of the droplet is large enough. Since the superfluid  $^4\text{He}$  core cannot be set into rotation around the symmetry axis because it is quantum-mechanically forbidden, all the angular momentum is stored in the  $^3\text{He}$  crust. This is in stark contrast with the case of pure  $^4\text{He}$  droplets, where oblate configurations can exist because they host quantized vortices.<sup>1,12,26</sup> In rotating mixed droplets, the  $^4\text{He}$  core may remain axisymmetric because the angular momentum is mainly stored in the  $^3\text{He}$  shell, which acts as a rotating deformable container. We have found that this happens up to the oblate-to-prolate bifurcation point at  $(\Lambda, \Omega) = (0.99, 0.52)$ , as shown in Fig. 1. Thus, for this composition, oblate stable configurations are vortex-free. We recall that for pure  $^3\text{He}$  droplets the bifurcation point is at  $(\Lambda, \Omega) = (1.28, 0.57)$ .<sup>5</sup>

In the prolate branch, the outer surface of the  $^3\text{He}$  crust is triaxial ellipsoid-like up to  $\Lambda \sim 1.64$ , where it becomes 2-lobed. At variance, the superfluid  $^4\text{He}$  core becomes 2-lobed at  $\Lambda \sim 1.05$ , i.e. immediately after bifurcation. This is due to the small surface tension of the  $^3\text{He}$ - $^4\text{He}$  interface,  $0.016 \text{ K}\text{\AA}^{-2}$ , as compared to that of the  $^3\text{He}$  free surface,  $0.113 \text{ K}\text{\AA}^{-2}$ . Pure  $^3\text{He}$  droplets become 2-lobed at  $\Lambda = 1.85$ .<sup>5</sup>

Prolate stable configurations with simply connected  $^4\text{He}$  cores have been found only in a narrow angular momentum range  $3.0 \leq \mathcal{L} \leq 3.5$ , where the core shape evolves from spheroidal to triaxial to 2-lobed. Due again to the small surface tension of the  $^3\text{He}$ - $^4\text{He}$  interface, the  $^4\text{He}$  core undergoes fission when the  $^3\text{He}$  crust is still triaxial ellipsoid-like. The resulting stable prolate configuration consist of a fissioned  $^4\text{He}$  core inside a rotating triaxial  $^3\text{He}$  crust. The transition from simply connected to fissioned  $^4\text{He}$  core configurations appears as a jump in

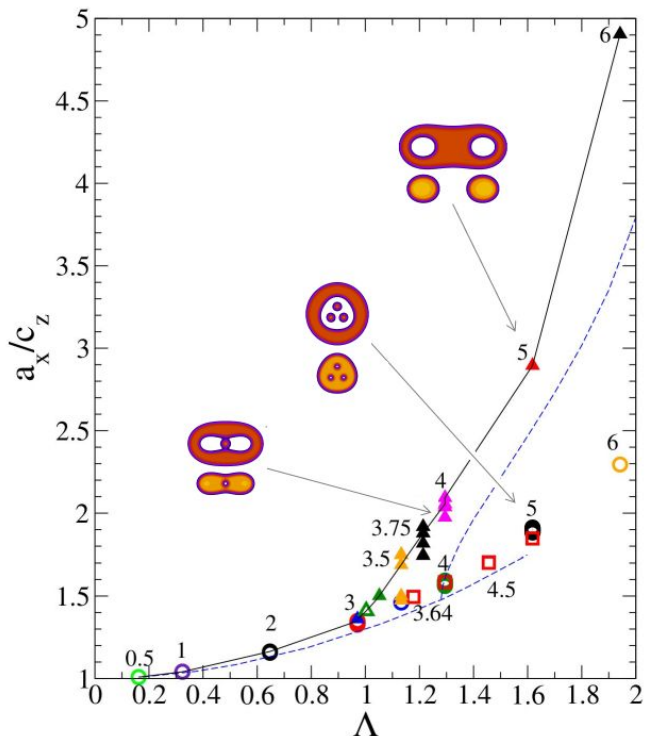


FIG. 3:  $a_x/c_z$  ratio of the outer  $^3\text{He}$  surface vs  $\Lambda$ . Symbols and lines have the same meaning as in Fig. 1. The numbers close to the symbols indicate the  $\mathcal{L}$  value. The pictograms represent calculated  $^3\text{He}$  (top) and  $^4\text{He}$  (bottom) 2D DFT densities for selected configurations.

the  $\Omega(\Lambda)$  curve on Fig. 1 at  $\Lambda = 1.31$ . Notice that the jump to fissioned inner  $^4\text{He}$  core (and the associated hysteresis loop as well) could not be predicted out of simple models based on energy minimization restricted to simply connected shapes.

We have looked for prolate configurations with a fissioned  $^4\text{He}$  core hosting a vortex in each moiety. After phase-imprinting them,<sup>1</sup> vortices are eventually expelled in the course of the numerical relaxation; we conclude that these configurations are not stable for up to the largest  $\Lambda$  addressed in this study,  $\Lambda = 1.97$ , a fairly large value for current experiments.

In spite of the fact that the lowest-energy configurations of the inner  $^4\text{He}$  droplet are mostly vortex-free (most of the angular momentum being efficiently stored in the  $^3\text{He}$  shell), we have found a number of vortex-hosting *metastable* configurations in our calculations. Remarkably, along the oblate branch (in the metastable region beyond the bifurcation point) we have found that configurations with  $n_v = 1$  have lower energy than vortex-free configurations. In this region, configurations hosting up to 4 vortices appear at  $\mathcal{L} > 3.5$ . All these configurations are metastable, as they may decay to prolate configurations lying at much lower energy (see Supplementary Table 1 for details).

In the oblate branch, we have also addressed multiply-

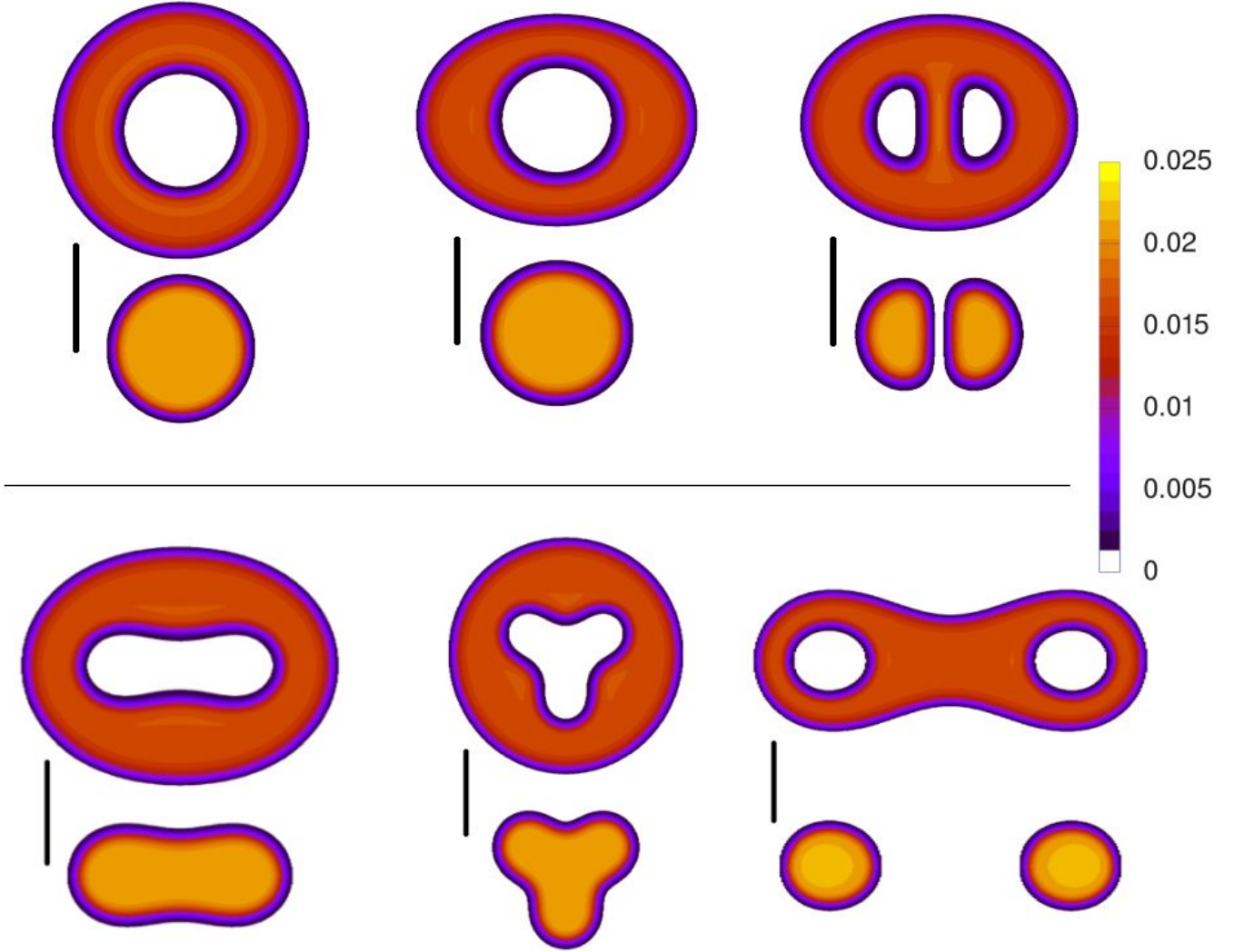


FIG. 4: Top: Density of the  ${}^4\text{He}_{1500}\text{-}{}^3\text{He}_{6000}$  droplet on a symmetry plane containing the rotational axis. From left to right, spherical configuration at  $\mathcal{L} = 0$ ; oblate vortex-free  ${}^4\text{He}$  core configuration at  $\mathcal{L} = 3$ , and oblate one-vortex configuration with quantum circulation  $m = 1$  at  $\mathcal{L} = 3$ . Bottom : Density of the  ${}^4\text{He}_{1500}\text{-}{}^3\text{He}_{6000}$  droplet on the symmetry plane perpendicular to the rotational axis. From left to right, prolate vortex-free  ${}^4\text{He}$  core configuration at  $\mathcal{L} = 3.5$ ; oblate 3-lobed  ${}^4\text{He}$  core configuration at  $\mathcal{L} = 4$ , and prolate fissioned  ${}^4\text{He}$  core configuration at  $\mathcal{L} = 6$ . For each configuration, the top density corresponds to the  ${}^3\text{He}$  crust and the bottom density to the  ${}^4\text{He}$  core. The black vertical bars represent a distance of 40 Å. The color bar shows the atom density in units of  $\text{\AA}^{-3}$  and is common to all configurations.

charged quantum vortices with charge (quantum circulation)  $m = 2 - 4$ , and their relative stability with respect to configurations with  $n_v = 2 - 4$  and  $m = 1$ . Multiply charged vortices in BEC have been found that are stabilized temporarily by the external confining potential.<sup>27,28</sup> In mixed helium droplets, the self-bound thick  ${}^3\text{He}$  shell yields a confining potential that plays the same role. We have found (see Supplementary Table 1) that, depending on  $\mathcal{L}$ , multiply charged single vortex configurations with charge  $m$  are more stable than  $n_v = m$  singly-charged vortices, and hence cannot decay into them as it would happen in pure  ${}^4\text{He}$ . This is likely due to the presence of  ${}^3\text{He}$  in the expanded vortex cores and the  ${}^3\text{He}$  crust, which together define a region similar to the rotating an-

nulus used to study quantized superfluid states and vortices in the first experiments on superfluid liquid  ${}^4\text{He}$ .<sup>29</sup>

Along the prolate branch, metastable  ${}^4\text{He}$  configurations with  $n_v = 1 - 2$  have been found (see Supplementary Table 1) where the angular momentum of the  ${}^4\text{He}$  core is shared between vortices and capillary waves as shown in Supplementary Fig. 3. This is similar to what happens in spinning  ${}^4\text{He}$  droplets.<sup>1,12</sup> When the  ${}^4\text{He}$  core becomes 2-lobed, the neck connecting them gets thinner as  $\mathcal{L}$  increases and eventually the most stable configuration is the fissioned one.

Three-lobed configurations were predicted to appear in classical droplets rotating at high velocities.<sup>3</sup> These configurations are metastable with respect to prolate 2-

lobed configurations and were not expected to be accessible experimentally. However, 3-lobed configurations were obtained,<sup>30</sup> stabilized by forcing the droplet into large amplitude periodic oscillations –thus not in gyrostatic equilibrium. Charged  $^4\text{He}$  drops magnetically levitated have been studied displaying  $\ell = 2$ -4 oscillation modes induced by a rotating deformation of the droplet.<sup>31</sup> More recently, triangular-shaped magnetically levitated water droplets have been found<sup>32</sup> where the amplitude of the surface oscillation is small and the equilibrium shape could be observed clearly for about 100 revolutions.

In the water droplet experiments, some surfactant was added to water to decrease the surface tension, helping the 3-lobed configurations to be formed. In the case of mixed helium droplets, the surface tension of the  $^3\text{He}$ - $^4\text{He}$  interface is already small, hence it is possible to have metastable 3-lobed  $^4\text{He}$  core configurations while the outer surface of the  $^3\text{He}$  crust is still oblate. Indeed, we have found such configurations in the  $3.64 \leq \mathcal{L} \leq 5$  range, one of which is shown in Fig. 4 (see also the central pictogram in Fig. 2). The 3-lobed bifurcation sets in at  $(\Lambda, \Omega) = (1.20, 0.58)$ . We have looked for metastable 4-lobed configurations but have not found any, the droplet always decaying into fissioned  $^4\text{He}$  prolate configurations.

### Discussion

The presence of a superfluid  $^4\text{He}$  core inside a normal fluid  $^3\text{He}$  droplet produces remarkable changes in its rotational properties. Oblate configurations are affected as the superfluid core cannot participate in the rotation because of its symmetry around the rotational axis. At variance with rotating pure  $^4\text{He}$  droplets, stable vortex-hosting oblate configurations are absent as it is energetically more favorable for the droplet to store angular momentum in the deformable  $^3\text{He}$  crust than in the superfluid  $^4\text{He}$  core. Vortex-hosting configurations are absent as equilibrium configurations in the prolate branch as well. While this could be due to the small size of the droplets studied here, it suggests that vortex-hosting stable configurations may be rare in large drops. We want to stress that, as Supplementary Table 1 shows, the energy difference between vortex-hosting and vortex-free configurations can be very small and likely separated by small energy barriers, so one should not discard that both types of configurations are found in actual experiments.

As for pure  $^4\text{He}$  droplets, the presence of vortices can be experimentally tested by doping the droplets with heliophilic impurities.<sup>9,12</sup> These impurities are captured by the droplet and sink into the  $^4\text{He}$  core.<sup>17</sup> Coherent x-ray scattering would reveal the space distribution of the impurities, which might arrange along the vortex cores if vortex arrays are present,<sup>9,12</sup> producing otherwise interference patterns very different from those of vortex-hosting droplets.

In the prolate branch, due to the small surface tension

of the  $^3\text{He}$ - $^4\text{He}$  interface, the  $^4\text{He}$  core fissions already at moderate angular velocities and superfluid, multiple cores configurations are the more stable ones. Diffractive imaging of multiple connected  $^4\text{He}$  cores for droplets of the size addressed in this work is challenging at present because they are small and the contrast is expected to be small, but likely not for the  $N = 10^8 - 10^{11}$  droplets in ongoing experiments.

It is less obvious whether metastable 3-lobed  $^4\text{He}$  core configurations may be experimentally detected; in the case of classical droplets, they were identified<sup>30,32</sup> twenty years after being predicted.<sup>3</sup> These configurations are highly unstable; for instance, Supplementary Table 1 shows that a clear 3-lobed configuration as that at  $\mathcal{L} = 4$  can either decay to the metastable oblate  $n_v = 1$  vortex configuration,  $\sim 8$  K below it, or to the stable prolate, fissioned core configuration, about 37 K below it.

An investigation on viscous immiscible two-fluid droplets has been conducted recently<sup>6</sup> that complements the present study on droplets made of two quantum fluids of limited solubility. Last but not least, our results can be used as benchmark for the applicability of these classical calculations to the quantum domain.

### Methods

We have considered in the present work mixed helium droplets at “zero temperature”, this meaning a temperature so low (a few mK) that thermal effects on the energetics and morphology of the droplet are negligible,  $^3\text{He}$  is in the normal phase, and  $^4\text{He}$  is superfluid.

The droplet is described within the DFT approach<sup>33</sup> using the density functional of Ref. 2. Due to the large number of  $^3\text{He}$  atoms in this study,  $^3\text{He}$  can be treated semiclassically in the Thomas-Fermi approximation.<sup>5</sup> The DFT equations have been solved adapting the 4He-DFT BCN-TLS computing package<sup>35</sup> to the case of helium mixtures. Further details are given in Supplementary Section 1.

### Code availability

The results have been obtained adapting the 4He-DFT BCN-TLS computing package which is freely available.<sup>35</sup>

### Acknowledgments

We are most indebted to Andrey Vilesov for informations on their ongoing experiments with mixed helium droplets that have motivated and clarified some aspects of this work, and to Sam Butler for useful exchanges. This work has been performed under Grant No FIS2017-87801-P (AEI/FEDER, UE). J.M.E. acknowledges support from Ministerio de Ciencia e Innovación of Spain through the Unidades de Excelencia “María



de Maeztu” grant MDM-2017-0767. M.B. thanks the Université Fédérale Toulouse Midi-Pyrénées for financial

support throughout the “Chaires d’Attractivité 2014” Programme IMDYNHE.

\* Electronic address: marti@fqa.ub.edu

- <sup>1</sup> R.A. Brown and L.E. Scriven, Proc. R. Soc. Lond. A **371**, 331 (1980).
- <sup>2</sup> J. Plateau, *Ann. Rep. of the Board of Regents of the Smithsonian Institution, Washington DC*, pp 207-285 (1863).
- <sup>3</sup> S. Chandrasekhar, Proc. R. Soc. London, Ser. A **286**, 1 (1965).
- <sup>4</sup> S. Cohen, R. Plasil, and W. J. Swiatecki, Ann. Phys. (NY) **82**, 557 (1974).
- <sup>5</sup> K.A. Baldwin, S.L. Butler, and R.J.A. Hill, Sci. Rep. **5**, 7660 (2015).
- <sup>6</sup> J. P. Toennies and A. F. Vilesov, Angew. Chem. Phys. **43**, 2622 (2004).
- <sup>7</sup> M. Hartmann, R. E. Miller, J. P. Toennies, and A. F. Vilesov, Phys. Rev. Lett. **75**, 1566 (1995).
- <sup>8</sup> B. G. Sartakov, J. P. Toennies, and A. Vilesov, J. Chem. Phys. **136**, 134316 (2012).
- <sup>9</sup> L.F. Gomez, K.R. Ferguson, J.P. Cryan, C. Bacellar, R.M.P. Tanyag, C. Jones, S. Schorb, D. Anielski, A. Belkacem, C. Bernando, R. Boll, J. Bozek, S. Carron, G. Chen, T. Delmas, L. Englert, S.W. Epp, B. Erk, L. Foucar, R. Hartmann, A. Hexemer, M. Huth, J. Kwok, S.R. Leone, J.H. S. Ma, F.R. N. C. Maia, E. Malmerberg, S. Marchesini, D.M. Neumark, B. Poon, J. Prell, D. Rolles, B. Rudek, A. Rudenko, M. Seifrid, K.R. Siefermann, F.P. Sturm, M. Swiggers, J. Ullrich, F. Weise, P. Zwart, C. Bostedt, O. Gessner, and A.F. Vilesov, Science **345**, 906 (2014).
- <sup>10</sup> B. Langbehn, K. Sander, Y. Ovcharenko, Ch. Peltz, A. Clark, M. Coreno, R. Cucini, M. Drabbels, P. Finetti, M. Di Fraia, L. Giannessi, C. Grazioli, D. Iablonskyi, A. C. LaForge, T. Nishiyama, V. Oliver Álvarez de Lara, P. Piseri, O. Plekan, K. Ueda, J. Zimmermann, K. C. Prince, F. Stienkemeier, C. Callegari, T. Fennel, D. Rupp, and T. Möller, Phys. Rev. Lett. **121**, 255301 (2018).
- <sup>11</sup> F. Ancilotto, M. Pi, and M. Barranco, Phys. Rev. B **97**, 184515 (2018).
- <sup>12</sup> S.M.O. O’Connell, R.M.P. Tanyag, D. Verma, Ch. Bernando, W. Pang, C. Bacellar, C.A. Saladrigas, J. Mahl, B.W. Toulson, Y. Kumagai, P. Walter, F. Ancilotto, M. Barranco, M. Pi, Ch. Bostedt, O. Gessner, and A.F. Vilesov, arXiv:1910.12926 (2019)
- <sup>13</sup> S. Erukala, D. Verma, S.M. O’Connell, A. Feinberg, C. Saladrigas, B. Toulson, M. Borgwardt, N. Shivaram, M.-F. Lin, A. Al Haddad, C. Bostedt, P. Walter, O. Gessner, and A. Vilesov, contribution to the Int. Conf. on Quantum Fluid Clusters QFC2019. [https://www.we-heraeus-stiftung.de/fileadmin/Redaktion/PDF/Seminare/2019/696\\_Booklet.pdf](https://www.we-heraeus-stiftung.de/fileadmin/Redaktion/PDF/Seminare/2019/696_Booklet.pdf).
- <sup>14</sup> M. Pi, F. Ancilotto, and M. Barranco, arXiv:1910.13187 (2019).
- <sup>15</sup> D.O. Edwards and M.S. Pettersen, J. Low Temp. Phys. **87**, 473 (1992).
- <sup>16</sup> S. Grebenev, J. P. Toennies, and A. F. Vilesov, Science **279**, 2083 (1998).
- <sup>17</sup> M. Barranco, R. Guardiola, S. Hernández, R. Mayol, J. Navarro, and M. Pi, J. Low Temp. Phys. **142**, 1 (2006).
- <sup>18</sup> F. Schreck, L. Khaykovich, K. L. Corwin, G. Ferrari, T. Bourdel, J. Cubizolles, and C. Salomon, Phys. Rev. Lett. **87**, 080403 (2001).
- <sup>19</sup> C.R. Cabrera, L. Tanzi, J. Sanz, B. Naylor, P. Thomas, P. Cheiney, and L. Tarruell, Science **359**, 301 (2018).
- <sup>20</sup> G. Semeghini, G. Ferioli, L. Masi, C. Mazzinghi, L. Wolswijk, F. Minardi, M. Modugno, G. Modugno, M. Inguscio, and M. Fattori, Phys. Rev. Lett. **120**, 235301 (2018).
- <sup>21</sup> D. Rakshit, T. Karpiuk, M. Brewczyk, and M. Gajda, SciPost Phys. **6**, 079 (2019).
- <sup>22</sup> D.S. Petrov, Phys. Rev. Lett. **115**, 155302 (2015).
- <sup>23</sup> S. Butler, Phys. Fluids **32**, 012115 (2020).
- <sup>24</sup> D.M. Jezek, M. Guilleumas, M. Pi, and M. Barranco, Phys. Rev. B **55**, 11092 (1997).
- <sup>25</sup> S.L. Butler, M.R. Stauffer, G. Sinha, A. Lilly, and R.J. Spiteri, J. Fluid Mech. **667**, 358 (2011).
- <sup>26</sup> F. Ancilotto, M. Pi, and M. Barranco, Phys. Rev. B **91**, 100503(R) (2015).
- <sup>27</sup> Y. Shin, M. Saba, M. Vengalattore, T. A. Pasquini, C. Sanner, A. E. Leanhardt, M. Prentiss, D. E. Pritchard, and W. Ketterle, Phys. Rev. Lett. **93**, 160406 (2004).
- <sup>28</sup> M. Okano, H. Yasuda, K. Kasa, M. Kumakura, and Y. Takahashi, J Low Temp. Phys. **148**, 447 (2007).
- <sup>29</sup> R.J. Donnelly, *Quantized vortices in Helium II* (Cambridge University Press, Cambridge, UK, 1991).
- <sup>30</sup> K. Ohsaka and E. H. Trinh, Phys. Rev. Lett. **84**, 1700 (2000).
- <sup>31</sup> D. L. Whitaker, M. A. Weilert, C. L. Vicente, H. J. Maris, and G. M. Seidel, J. Low Temp. Phys. **110**, 173 (1998).
- <sup>32</sup> R. J. A. Hill and L. Eaves, Phys. Rev. Lett. **101**, 234501 (2008).
- <sup>33</sup> F. Ancilotto, M. Barranco, F. Coppens, J. Eloranta, N. Halberstadt, A. Hernando, D. Mateo, and M. Pi, Int. Rev. Phys. Chem. **36**, 621 (2017).
- <sup>34</sup> M. Barranco, M. Pi, S.M. Gatica, E.S. Hernández, and J. Navarro, Phys. Rev. B **56**, 8997 (1997).
- <sup>35</sup> 4He-DFT BCN-TLS: A Computer Package for Simulating Structural Properties and Dynamics of Doped Liquid Helium-4 Systems. M. Pi, F. Ancilotto, F. Coppens, N. Halberstadt, A. Hernando, A. Leal, D. Mateo, R. Mayol, and M. Barranco, <https://github.com/bcntls2016/>.

## Supplementary Information for “Rotating mixed $^3\text{He}$ - $^4\text{He}$ nanodroplets”

### S1.- The DFT approach for mixed $^3\text{He}$ - $^4\text{He}$ droplets

The DFT equations obtained by functional variation of the energy density are formulated in a rotating frame of reference with constant angular velocity  $\omega$  around the  $z$  axis.<sup>1</sup> In terms of the DFT Hamiltonians  $\mathcal{H}_3[\rho_3, \rho_4]$  and  $\mathcal{H}_4[\rho_3, \rho_4]$ ,<sup>2</sup>

$$\left\{ \mathcal{H}_3[\rho_3, \rho_4] - \frac{m_3}{2} \omega^2 (x^2 + y^2) \right\} \Psi_3(\mathbf{r}) = \mu_3 \Psi_3(\mathbf{r})$$

$$\left\{ \mathcal{H}_4[\rho_3, \rho_4] - \omega \hat{L}_4 \right\} \Psi_4(\mathbf{r}) = \mu_4 \Psi_4(\mathbf{r}) \quad (1)$$

where  $\mu_3(\mu_4)$  is the  $^3\text{He}$ ( $^4\text{He}$ ) chemical potential,  $\hat{L}_4$  is the  $^4\text{He}$  angular momentum operator, and  $\Psi_3(\mathbf{r})$  and  $\Psi_4(\mathbf{r})$  are the real  $^3\text{He}$  and complex  $^4\text{He}$  effective wavefunctions related to the atom densities as  $\Psi_3^2(\mathbf{r}) = \rho_3(\mathbf{r})$  and  $|\Psi_4(\mathbf{r})|^2 = \rho_4(\mathbf{r})$ . These equations are solved imposing a given value of the total angular momentum per atom, which requires finding iteratively the value of  $\omega$ . Classically, this corresponds to torque-free droplets with an initially prescribed rotation, as they are isolated.

Vortices are nucleated in the  $^4\text{He}$  core using the imprinting procedure<sup>1</sup> by which  $n_v$  vortex lines parallel to the  $z$  axis are initially created, *i.e.*, one starts the iterative solution of Eq. (1) from the wave function

$$\Psi_4(\mathbf{r}) = \sqrt{\tilde{\rho}_4(\mathbf{r})} \prod_{j=1}^{n_v} \frac{(x - x_j) + i(y - y_j)}{\sqrt{(x - x_j)^2 + (y - y_j)^2}} \quad (2)$$

where  $(x_j, y_j)$  is the initial position of the  $j$ -vortex linear core with respect to the  $z$ -axis of the droplet, and  $\tilde{\rho}_4(\mathbf{r})$  is the vortex-free  $^4\text{He}$  density. The initial vortex positions are guessed and during the functional minimization of the total energy, both the vortex positions and droplet density are allowed to change to provide at convergence the lowest energy configuration for the chosen value of  $L_z$ .

### S2.- Scaled angular momentum and angular velocity

Classical rotating droplets subject to surface tension and centrifugal forces are characterized by two dimen-

sionless variables, angular momentum  $\Lambda$  and velocity  $\Omega$  that allow to describe the sequence of droplet shapes in a universal phase diagram, independently of the droplet size.<sup>3,4</sup> These variables have been used to characterize pure  $^4\text{He}$  and  $^3\text{He}$  droplets within the DFT approach.<sup>1,5</sup>

The definitions of  $\Lambda$  and  $\Omega$  have been generalized to the case of droplets made of two immiscible fluids as follows.<sup>6</sup> An effective particle density  $\rho_{\text{eff}}$  and mass  $m_{\text{eff}}$  are introduced such that the moment of inertia of a spherical droplet with such effective mass and density coincides with that of a spherical droplet of inner radius  $R_i$  and atom density  $\rho_4$  surrounded by a spherical shell of outer radius  $R_o$  and atom density  $\rho_3$ :

$$m_{\text{eff}} \rho_{\text{eff}} = \frac{m_4 \rho_4 R_i^5 + m_3 \rho_3 (R_o^5 - R_i^5)}{R_o^5} \quad (3)$$

together with an effective surface tension

$$\gamma_{\text{eff}} = \frac{\gamma_{34} R_i + \gamma_3 R_o}{R_o} \quad (4)$$

where  $\gamma_{34}$  is the surface tension of the  $^3\text{He}$ - $^4\text{He}$  interface and  $\gamma_3$  that of the  $^3\text{He}$  free surface. The scaled variables  $\Lambda$  and  $\Omega$  are then written as for pure droplets<sup>3,4</sup> but replacing  $m$  and  $\gamma$  with  $m_{\text{eff}}$  and  $\gamma_{\text{eff}}$ , respectively:

$$\Lambda = \frac{N \hbar}{\sqrt{8 \gamma_{\text{eff}} R_o^7 m_{\text{eff}} \rho_{\text{eff}}}} \mathcal{L} \quad (5)$$

$$\Omega = \sqrt{\frac{m_{\text{eff}} \rho_{\text{eff}} R_o^3}{8 \gamma_{\text{eff}}}} \omega. \quad (6)$$

Note that  $\Lambda$  is written in terms of the total angular momentum per atom in  $\hbar$  units,  $\mathcal{L} = (L_3 + L_4)/(N_3 + N_4) = L/N$ .

The values of the magnitudes entering the above equations are:  $\gamma_3 = 0.113 \text{ K } \text{\AA}^{-2}$ ,  $\gamma_{34} = 0.016 \text{ K } \text{\AA}^{-2}$ ,  $\hbar^2/(2m_3) = 8.0418 \text{ K } \text{\AA}^2$ ,  $\hbar^2/(2m_4) = 6.0597 \text{ K } \text{\AA}^2$ ,  $\rho_3 = 0.016347 \text{ \AA}^{-3}$ , and  $\rho_4 = 0.021836 \text{ \AA}^{-3}$ . For the  $N_3 = 6000$ ,  $N_4 = 1500$  droplet, one gets  $R_i = 25.40 \text{ \AA}$  and  $R_o = 47.02 \text{ \AA}$ , and hence  $\Lambda = \mathcal{L}/3.042$  and  $\Omega = 10.61 \hbar \omega$ , if  $\hbar \omega$  is given in K.

\* Electronic address: marti@fqa.ub.edu

<sup>1</sup> F. Ancilotto, M. Pi, and M. Barranco, Phys. Rev. B **97**, 184515 (2018).

<sup>2</sup> M. Barranco, M. Pi, S.M. Gatica, E.S. Hernández, and J. Navarro, Phys. Rev. B **56**, 8997 (1997).

<sup>3</sup> R.A. Brown and L.E. Scriven, Proc. R. Soc. Lond. A **371**,

331 (1980).

<sup>4</sup> S.L. Butler, M.R. Stauffer, G. Sinha, A. Lilly, and R.J. Spiteri, J. Fluid Mech. **667**, 358 (2011).

<sup>5</sup> M. Pi, F. Ancilotto, and M. Barranco, arXiv:1910.13187 (2019).

<sup>6</sup> S. Butler, Phys. Fluids **32**, 012115 (2020).

	$\Lambda$	$\Omega$	$\mathcal{L}$ ( $\hbar$ )	$\mathcal{L}_3$ ( $\hbar$ )	$\mathcal{L}_4$ ( $\hbar$ )	$\hbar\omega$ ( $\times 10^{-2}\text{K}$ )	$\mathcal{R}$ (K)	$^3\text{He}$					$^4\text{He}$		
								$a_x$ ( $\text{\AA}$ )	$b_y$ ( $\text{\AA}$ )	$c_z$ ( $\text{\AA}$ )	$a_x/c_z$	$b_y^3/V$	$a_x$ ( $\text{\AA}$ )	$b_y$ ( $\text{\AA}$ )	$c_z$ ( $\text{\AA}$ )
<u><b>O</b></u>	0.164	0.105	0.5	0.50	0.00	0.99	-22488.5	47.36	47.36	46.95	1.009	0.243	25.29	25.26	25.35
<u><b>O</b></u>	0.329	0.206	1	1.00	0.00	1.94	-22433.3	47.86	47.86	45.96	1.041	0.251	25.24	25.22	25.43
O1v	0.329	0.169	1	0.80	0.20	1.59	-22385.4	47.87	47.87	45.93	1.042	0.251	29.15	29.15	—
<u><b>O</b></u>	0.657	0.381	2	2.00	0.00	3.59	-22223.4	49.64	49.63	42.65	1.164	0.280	25.26	25.19	25.31
O1v	0.657	0.352	2	1.80	0.20	3.32	-22198.8	49.49	49.49	42.81	1.156	0.278	28.90	28.90	—
<u><b>O</b></u>	0.986	0.517	3	3.00	0.00	4.87	-21903.87	52.02	52.02	38.57	1.349	0.322	25.57	25.57	24.31
O1v	0.986	0.493	3	2.80	0.20	4.65	-21897.4	51.83	51.83	38.57	1.344	0.319	28.67	28.67	—
O1v2m	0.986	0.474	3	2.60	0.40	4.47	-21875.2	51.67	51.67	38.77	1.333	0.316	32.59	32.59	—
O1v3m	0.986	0.451	3	2.40	0.60	4.25	-21851.2	51.61	51.61	38.90	1.327	0.315	35.77	35.77	—
O	1.151	0.571	3.5	3.50	0.00	5.38	-21711.4	53.33	53.33	36.50	1.461	0.347	25.89	25.89	23.47
O1v	1.151	0.550	3.5	3.50	0.20	5.18	-21713.0	53.12	53.12	36.33	1.462	0.343	28.67	28.67	—
O1v2m	1.151	0.533	3.5	3.10	0.40	5.02	-21697.0	52.93	52.93	36.51	1.449	0.339	32.48	32.48	—
O	1.315	0.618	4	4.00	0.00	5.82	-21501.1	54.66	54.66	34.48	1.585	0.374	26.36	26.36	22.47
O1v	1.315	0.597	4	3.80	0.20	5.63	-21510.2	54.46	54.46	34.17	1.594	0.370	28.80	28.80	—
O1v2m	1.315	0.582	4	3.60	0.40	5.49	-21499.8	54.27	54.27	34.26	1.584	0.366	32.42	32.42	—
O1v3m	1.315	0.568	4	3.40	0.60	5.35	-21488.6	54.10	54.10	34.43	1.571	0.363	35.73	35.73	—
O1v4m	1.315	0.550	4	3.20	0.80	5.18	-21474.8	54.01	54.01	34.59	1.561	0.361	38.38	38.38	—
O2v	1.315	0.589	4	3.70	0.30	5.56	-21496.8	54.18	54.26	34.62	1.565	0.366	30.87	29.23	18.72
O1v	1.644	0.673	5	4.80	0.20	6.34	-21059.9	57.17	57.17	30.10	1.899	0.428	29.42	29.42	—
O1v2m	1.644	0.660	5	4.60	0.40	6.22	-21059.4	56.99	56.99	29.87	1.908	0.424	32.56	32.56	—
O1v3m	1.644	0.648	5	4.40	0.60	6.11	-21057.0	56.81	56.81	29.93	1.898	0.420	35.76	35.76	—
O1v4m	1.644	0.637	5	4.20	0.80	6.00	-21053.5	56.65	56.65	30.08	1.883	0.416	38.55	38.55	—
O2v	1.644	0.660	5	4.63	0.37	6.22	-21057.7	57.27	56.76	29.94	1.913	0.419	33.73	30.13	—
O3v	1.644	0.650	5	4.50	0.50	6.13	-21050.2	56.88	56.89	30.01	1.895	0.422	34.36	34.30	3.05
O4v	1.644	0.644	5	4.39	0.61	6.07	-21039.6	56.77	56.77	30.14	1.884	0.419	36.47	36.47	11.80
O4v	1.972	0.696	6	5.39	0.71	6.56	-20565.5	59.44	59.44	25.90	2.295	0.481	38.13	38.13	7.34
3L	1.197	0.584	3.64	3.628	0.008	5.50	-21655.7	53.74	53.62	35.94	1.495	0.353	—	—	—
3L	1.315	0.607	4	3.880	0.120	5.72	-21502.4	54.44	54.68	34.37	1.584	0.374	—	—	—
3L	1.479	0.638	4.5	4.278	0.222	6.01	-21282.9	54.79	56.85	32.20	1.702	0.421	—	—	—
3L	1.644	0.655	5	4.541	0.459	6.17	-21056.0	55.63	58.28	30.12	1.847	0.453	—	—	—
P	0.986	0.516	3	2.994	$6.3 \times 10^{-3}$	4.86	-21903.86	52.51	51.54	38.57	1.361	0.313	27.83	23.36	24.22
<u><b>P</b></u>	1.019	0.523	3.1	3.060	0.040	4.93	-21867.1	53.78	50.72	38.13	1.410	0.299	31.38	20.20	23.62
<u><b>P</b></u>	1.052	0.528	3.2	3.116	0.084	4.98	-21829.9	55.34	49.64	37.69	1.468	0.280	34.17	18.05	22.85
<u><b>P</b></u>	1.068	0.529	3.25	3.141	0.109	4.99	-21811.2	56.27	48.96	37.47	1.502	0.269	35.51	17.18	22.39
<u><b>P</b></u>	1.151	0.523	3.5	3.264	0.236	4.93	-21718.0	61.37	45.20	36.31	1.690	0.211	41.44	14.46	19.94
P1v	1.151	0.549	3.5	3.299	0.201	5.17	-21712.9	54.52	51.73	36.34	1.500	0.317	29.39	27.97	—
P2v	1.151	0.544	3.5	3.239	0.261	5.12	-21697.7	53.78	52.31	36.47	1.475	0.328	30.95	29.93	—
Pf	1.151	0.483	3.5	2.897	0.603	4.55	-21705.5	63.24	43.04	36.14	1.750	0.183	—	—	—
<u><b>P</b></u>	1.233	0.506	3.75	3.385	0.365	4.77	-21627.0	66.12	41.90	35.18	1.879	0.168	46.69	12.94	17.47
P1v	1.233	0.528	3.75	3.488	0.262	4.98	-21617.4	63.96	44.00	35.20	1.817	0.195	37.43	22.87	—
P2v	1.233	0.528	3.75	3.329	0.421	4.98	-21603.1	61.76	45.70	35.40	1.745	0.219	41.05	23.98	14.27
Pf	1.233	0.470	3.75	3.003	0.747	4.43	-21621.6	67.08	40.53	34.98	1.918	0.152	52.74	—	—
P	1.315	0.488	4	3.499	0.501	4.60	-21539.1	70.04	39.35	34.08	2.055	0.139	51.45	11.65	15.04
P1v	1.315	0.492	4	3.422	0.578	4.64	-21527.8	69.08	40.00	34.13	2.024	0.091	51.06	13.76	—
P2v	1.315	0.498	4	3.389	0.611	4.69	-21512.3	67.75	41.10	34.31	1.975	0.159	49.41	19.45	11.31
<u><b>Pf</b></u>	1.315	0.455	4	3.115	0.885	4.29	-21539.8	70.77	38.20	33.80	2.094	0.128	—	—	—
<u><b>Pf</b></u>	1.644	0.386	5	3.640	1.360	3.64	-21242.8	83.55	30.56	28.86	2.895	0.065	—	—	—
<u><b>Pf</b></u>	1.972	0.385	6	4.317	1.683	2.69	-20999.7	97.61	20.19	19.90	4.905	0.019	—	—	—

TABLE I: Characteristics of the rotating  $^3\text{He}_{6000}$ - $^4\text{He}_{1500}$  droplet ( $x_3 = 80\%$ ). O: oblate configurations; P: prolate configurations; 3L: 3-lobed  $^4\text{He}$  core configurations (the outer surface of the  $^3\text{He}$  crust is sensibly oblate); Pf: fissioned  $^4\text{He}$  core configurations. “1v3m” e.g., means 1 vortex with circulation (charge) 3.  $\mathcal{L} = \mathcal{L}_3 + \mathcal{L}_4 = L_3/N + L_4/N$  with  $N = N_3 + N_4$ , and  $V$  is the volume of the spherical droplet at rest. The most stable configuration for each  $\mathcal{L}$  value is underlined boldface. Some entries are empty because they are not well defined or meaningless.



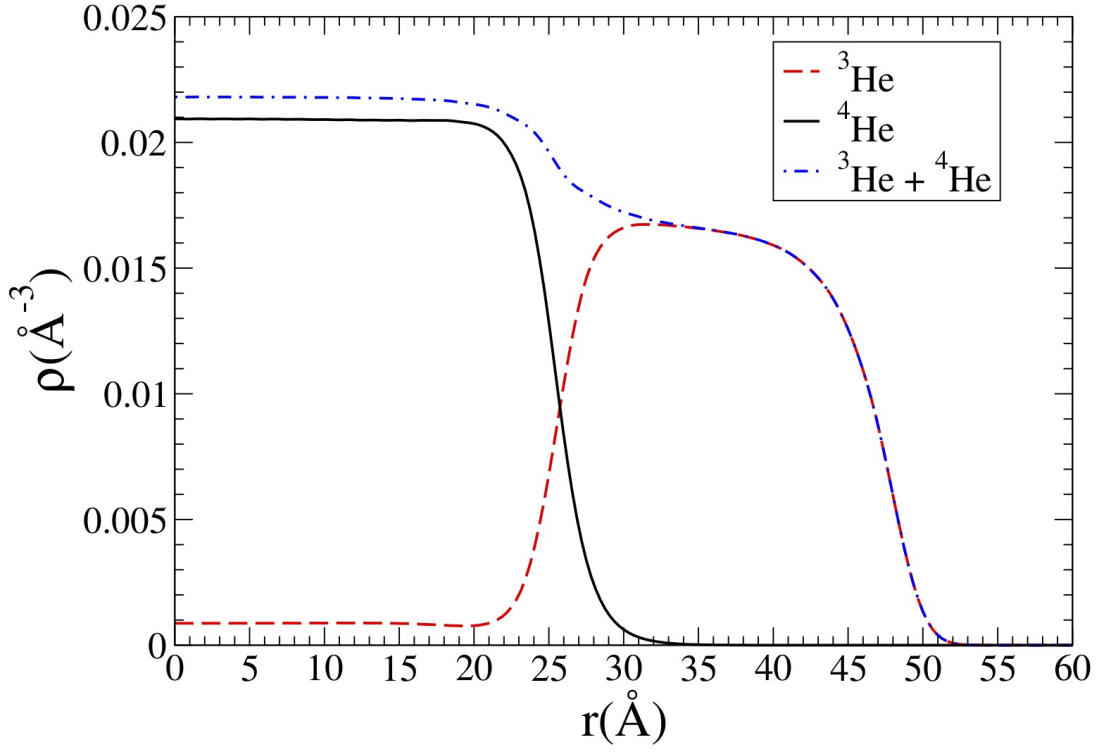


FIG. 5: Density profile of the spherical  ${}^4\text{He}_{1500} + {}^3\text{He}_{6000}$  droplet as a function of the distance to the droplet center.

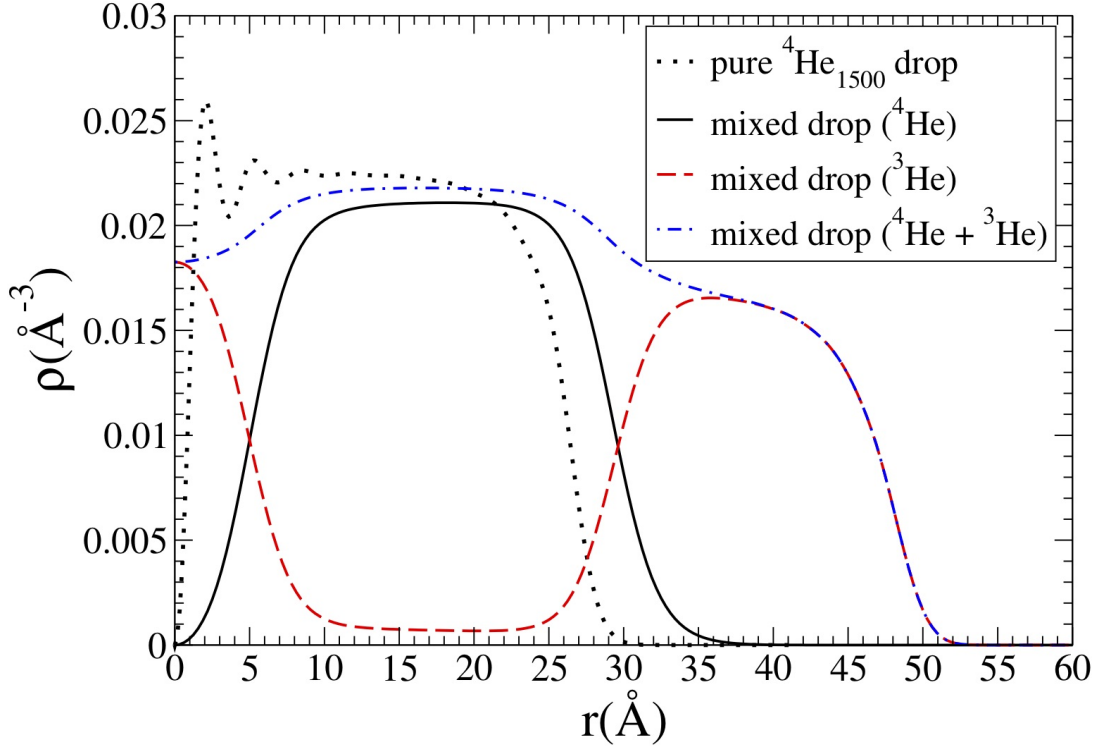


FIG. 6: Comparison between the density profile of the pure  ${}^4\text{He}_{1500}$  droplet and that of the  ${}^4\text{He}$  core of the  ${}^4\text{He}_{1500} + {}^3\text{He}_{6000}$  mixed droplet. Both droplets host a vortex line. In the later case the density profile of the  ${}^3\text{He}$  component is also shown. Densities are shown along the radial direction within the symmetry plane perpendicular to the vortex line.